UNSTEADY FLOW EVOLUTION AND FLAME DYNAMICS IN A LEAN-PREMIXED SWIRL-STABILIZED COMBUSTOR

Ying Huang and Vigor Yang
Department of Mechanical Engineering
The Pennsylvania State University
University Park, PA 16802, *USA*
huangying@psu.edu; vigor@psu.edu

ABSTRACT

A comprehensive numerical analysis has been conducted to study the unsteady flow evolution and flame dynamics in a lean-premixed (LPM) swirl-stabilized combustor using a large-eddy-simulation (LES) technique along with a level-set flamelet library approach. Emphasis is placed on the key mechanisms and operation parameters responsible for driving combustion oscillations. Results indicate that the inlet air temperature and equivalence ratio are the two most important parameters determining the stability characteristics of the LPM combustor. A slight increase in the inlet air temperature across the stability boundary leads to a transition from a stable to an unstable flame and consequently a sudden increase in acoustic flow oscillation. Several prevailing processes involved in the flame bifurcation phenomenon are identified and quantified. In addition, the mutual coupling between the heat release in the flame zone and the flow development is carefully examined under both stable and unstable operating conditions.

INTRODUCTION

The increasingly strict regulation of pollutant emissions has recently urged engine manufactures to turn to the concept of lean premixed (LPM) combustion as an effective means to fulfill the regulatory requirements (Correa, 1993; Lefebvre, 1995). However, combustion instabilities or unsteady flow oscillations have often emerged as a common problem hindering the development of LPM combustors. Although several mechanisms responsible for initiating and sustaining combustion instabilities, such as hydrodynamic instabilities and equivalence-ratio fluctuations have been proposed and studied (Schadow and Gutmark, 1992, Lieuwen and Zinn, 1998), quantitative understanding of the physiochemical processes and operating parameters dictating the occurrence of instabilities is far from completion. The situation is further complicated when LPM systems use swirling flow to stabilize the flame with recirculation, which produces a relative compact flame and increases the susceptibility to combustion instability. Fundamental investigations into this issue are strongly needed to further improve our knowledge of combustion instabilities.

Many experimental works (Knoop et al., 1997, Broda et al., 1998, Johnson et al., 2000, Lee et al., 2000, etc.) have been conducted to investigate the combustion dynamics in LPM combustors. A notable example is the configuration reported by Broda et al. (1998) and Seo (1999). The system consists of a single-swirl injector, an axisymmetric chamber, and a choked nozzle, as shown schematically in Fig.1. The estimated swirl number is 0.76 for a 45-degree swirler with a constant chord (c) and angle (φ). Natural gas is injected radially from the center body through ten holes immediately downstream of the swirler vanes. The fuel/air mixture is assumed to be well mixed before entering the combustor. A broad range of the equivalence ratio and inlet air temperature was considered systematically. It was found that instabilities take place only if the inlet air temperature is greater that a threshold value T_{in}^{*} around 660 K and the equivalence ratio falls into the range between 0.5 and 0.7. As the inlet temperature increases and exceeds the threshold value T_{in}^{*}, the flame bifurcates from a stable state (characterized by a limit cycle with small oscillation) to an unstable state (characterized by a limit cycle with large oscillation). The present numerical study attempts to address this bifurcation phenomenon in flame structure and to investigate the key mechanisms and operation parameters responsible for initiating and sustaining combustion oscillations.

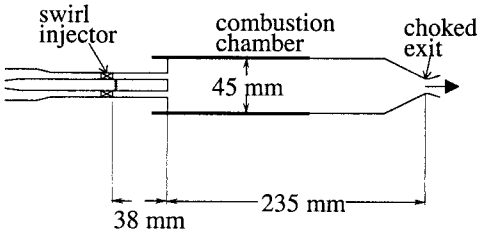

Fig. 1 Schematic of a model swirl-stabilized combustor (Broda, et al., 1998)

THEORETICAL FORMULATION AND NUMERICAL METHOD

The formulation is based on the Favre-filtered conservation equations of mass, momentum and energy in three dimensions. The subgrid-scale (*sgs*) terms is modeled using the compressible-flow version of the Smagorinsky model suggested by Erlebacher et al. (1992). The damping function of Van-Driest is used to take into account the inhomogeneities near the wall. For treating turbulent combustion within the context of LES, combustion models are often needed on the sub-grid scales. The level-set flamelet library approach, which has been successfully applied to study premixed turbulent combustion (Pitsch, 2002, Huang, et al., 2003a, Huang and Yang, 2003b), is used here.

Proceeding of Third International Symposium on Turbulent and Shear Flow Phenomena

Boundary conditions must be specified to complete the formulation. The no-slip and adiabatic conditions are enforced along all of the solid walls. At the inlet boundary, the mass flow rate and temperature are specified. The pressure is obtained from a one-dimensional approximation to the axial momentum equation, i.e., $\partial p/\partial x + \rho u \partial u/\partial x = 0$. The inlet velocity profiles are obtained from the mass flow rate, density, and swirler vane angle. Turbulent disturbances with an intensity of 15% of the mean-flow quantities are imposed using a Gaussian random number generator. At the outlet boundary, the characteristic conditions proposed by Poinsot and Lele (1992) are applied, along with the specification of a time-invariant back pressure because there exists an acoustic pressure node at the middle of the chamber and the computational domain only includes the upstream half of the chamber. This back pressure is obtained using a simplified one-dimensional momentum equation $\partial p/\partial r = \rho U_\theta^2/r$ in the radial direction, where U_θ is mean azimuthal velocity. The pressure at $r = 0$ is fixed as a pre-specified value.

The resultant governing equations and boundary conditions are solved numerically by means of a density-based, finite-volume methodology. The spatial discretization employs a second-order, central-differencing method in generalized coordinates. A fourth-order matrix dissipation with a total-variation-diminishing (TVD) switch developed by Swanson & Turkel (1992) and tested by Oefelein & Yang (1998) is employed to ensure computational stability and to prevent numerical oscillations in regions with steep gradients. Temporal discretization is obtained using a four-step Runge-Kutta integration scheme. A multi-block domain decomposition technique along with static load balance is used to facilitate the implementation of parallel computation with message passing interface at the domain boundaries. The theoretical and numerical framework described above has been validated by Apte & Yang (2001) and Huang et al.(2003a, 2003b) against a wide variety of flow problems in order to establish its creditability and accuracy.

RESULTS AND DISCUSSION

The model combustor described in the preceding section is treated in the present work. The chamber measures a diameter of 45 *mm* and a length of 235 *mm*. The baseline condition includes an equivalence ratio of 0.573 and a chamber pressure of 0.463 *Mpa*. The mass flow rates of the natural gas and air are 1.71 and 50.70 *g/s*, respectively. The inlet flow velocity is 86.6 *m/s* and the corresponding Reynolds number based on the flow velocity and height of the inlet annulus is 35000.

The computational domain includes the upstream half of the chamber and part of the inlet annulus. The entire grid system has 176x141x81 points along the axial, radial, and azimuthal directions, respectively, of which 36 axial points are used to cover the inlet section. The grids are clustered in the shear-layer regions downstream of the dump plane and near the solid walls. The largest grid size falls in the inertial range of the turbulent energy spectrum based on the inlet Reynolds number. The computational domain is divided into 68 blocks and the analysis is conducted on a distributed-memory parallel computer with each block calculated on a single processor.

Stable Flame Dynamics

Stable flame evolution is first obtained for the inlet air temperature of 600 *K* (below the threshold value T_{in}^* for the onset of combustion oscillation). The flame bifurcation phenomenon is then investigated by increasing the inlet air temperature from 600 to 660 *K*. Figure 2 shows the mean temperature contours and pseudo-streamlines on the $x-r$ plane based on the mean axial and radial velocity components for a stable flame. A torodial recirculation zone (CRTZ) is established in the wake of the center body under the effects of the swirling flow. The CTRZ, a form of vortex breakdown, serves as a flame stabilization region where hot products are mixed with the incoming mixture of air and fuel. In addition, as a result of the sudden enlargement of the combustor configuration, a corner recirculation zone (CRZ) is formed downstream of the backward-facing step.

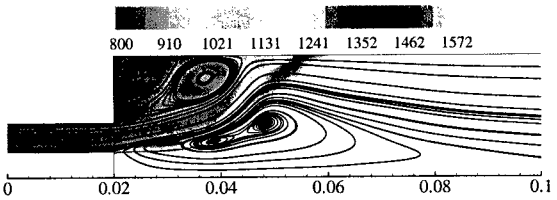

Fig. 2 Mean temperature contours and streamlines of stable flame

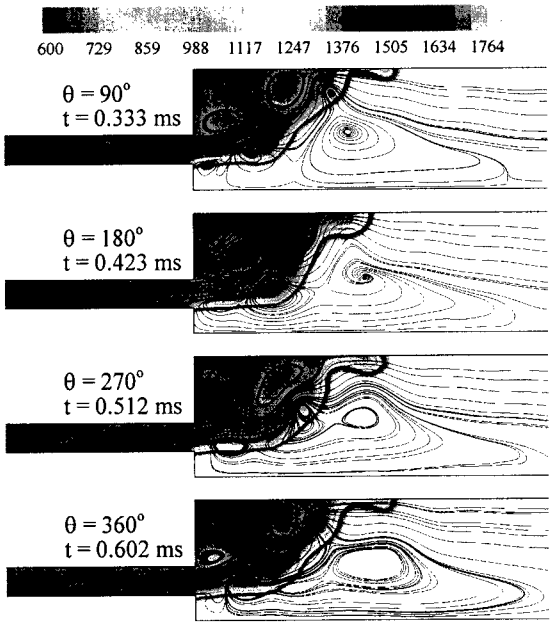

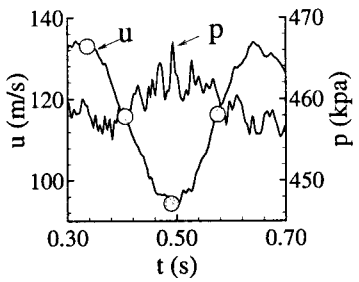

Fig. 3 Stable flame evolution over one cycle of oscillation (3214*Hz*): temperature contours and streamlines.

The calculated pressure and velocity fluctuations show the existence of a dominant harmonic mode at 3214 *Hz*, corresponding to the frequency of the vortex shedding from the center body. Figure 3 presents the flame evolution and vortex shedding process in the upstream region of the chamber over one cycle of oscillation. The phase angle θ is referenced with respect to the acoustic velocity at the chamber head-end. The entire process is dictated by the temporal evolution and spatial distribution of the flame front, which moves periodically under the effects of the vortical flow motion (indicated by the concentrated streamlines) in the chamber. A new vortex begins to shed from the center body at $\theta = 90^0$, accompanying with a higher speed mixture. As the vortex proceeds downstream ($\theta = 180^0$ - 270^0), it distorts the flame front and even produces a separated flame pocket. At the same time, the higher speed mixture arising from the local acoustic motion pushes the flame downstream. When the vortex moves away from the flame ($\theta = 360^0$) and dissipates into small-scale structures, the flame front propagates upstream and interacts with another incoming vortex. During this process, a new vortex appears at the corner of the center body and another cycle repeats.

Bifurcation of Flame Structure

The inlet air temperature has enormous effects on the flame dynamics. On the one hand, when the inlet air temperature increases, for a fixed mass flow rate, it will increase the flow velocity and push the flame downstream. On the other hand, the increased inlet air temperature leads to an increase in the flame speed, and consequently renders the flame to propagate upstream. In addition, flashback may occur near the wall due to the small local flow velocity. The combined effects of flow acceleration, flame-speed enhancement, and flashback will determine the final form of the flame structure.

In the present study, as the inlet air temperature increases abruptly from 600 to 660 K, flame bifurcation takes place. The flame originally anchored in the center recirculation zone penetrates into the corner recirculation zone and flashes back. Consequently, the flame is stabilized by both the corner- and center-recirculating flows and forms a compact enveloped configuration. The flame flaps dynamically and drives flow oscillations through its influence on unsteady heat release. And at the same time, the pressure oscillation in the chamber increases and reaches another limit cycle with a much larger amplitude. The entire bifurcation process can be divided into three stages: high-temperature mixture filling process, flame trapping process, and vortex flashback process, as shown in Fig. 4.

Figures 4a-4c show the high-temperature mixture filling process. As the inlet mixture temperature increases, the flow speed increases due to the decreased density for a fixed mass flow rate. As a result, the original low-temperature mixture is pushed downstream toward the flame. Although a flashback phenomenon is observed near the wall, the high-temperature mixture hasn't reached the flame front near the wall, the flame speed remains unchanged at this stage.

Figures 4d-4e show the flame trapping process. After the high-temperature mixture reaches the flame front, with the help of the increased flame speed, the near-wall flashback overcomes the flow acceleration effects. Consequently, the flame front penetrates into the corner recirculation zone and is trapped by the local vortical motion.

In the vortex flashback process shown in Figs. 4f-4h, the flame propagates upstream under the influence of the vortical motion. A counter-clockwise vortex originally shed from the tip of the backward step approaches and pushes the flame front in the corner recirculation zone further toward the dump plane. At the same time, a small flame pocket is produced and separated from the main mixture stream. After the vortex is convected downstream and passes through the flame, another vortex approaches and interacts with the flame. This process continues and eventually the fresh reactant in the corner recirculation zone is completely consumed by chemical reactions. The flame is stabilized by both the corner- and center-recirculating flows.

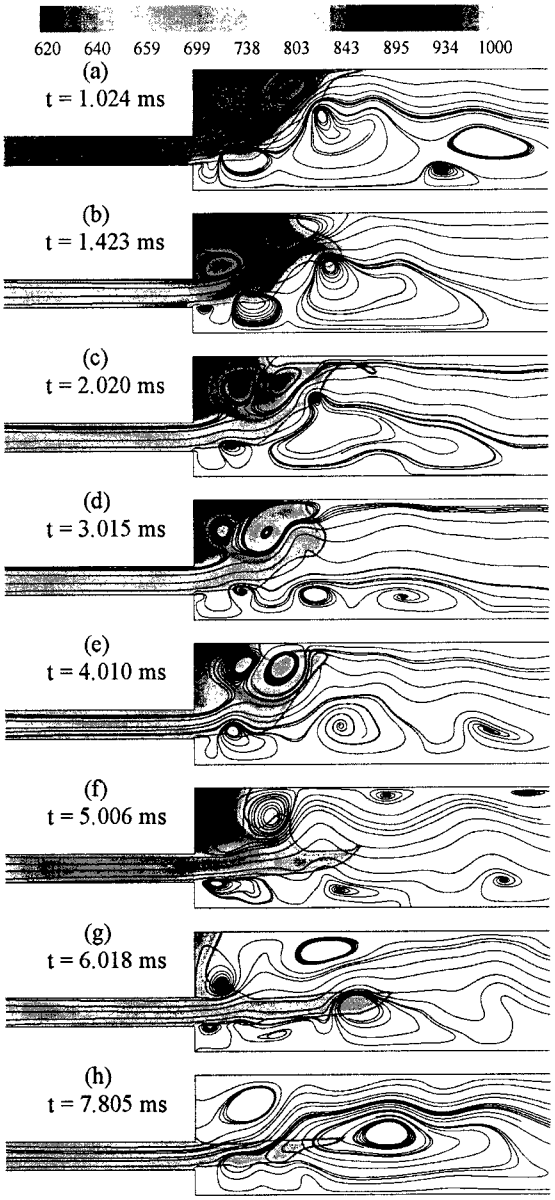

Fig. 4 Transition from stable to unstable flame with increased inlet temperature from 600 to 660 K.

In light of the above observation, we conclude that the flashback phenomenon dictates the flame bifurcation process. The occurrence of flashback is usually attributed to

two mechanisms. The first involves flame propagation in the boundary layer along a solid wall where the local velocity diminishes toward the surface. The second mechanism is associated with flow reversal, which is usually caused by vortical motions or acoustics oscillations. Both mechanisms are observed in the present case. A criterion for the occurrence of near-wall flashback, valid for both adiabatic and isothermal walls, was recently proposed by Kurdyumov et al.(2000). Flashback occurs if the Karlovitz number, defined as $\alpha A / S_L^2$ with α being the thermal diffusivity and A the velocity gradient at the wall, is less than a critical value. Although this criterion is formulated for laminar flows, the result is qualitatively applicable for flames in turbulent boundary layers. In the present case, the flame speed increases as the inlet air temperature increases. Consequently, the flame is more prone to flashback through the wall boundary layers according to Kurdyumov's criterion. Flashback arising from local flow reversal has also been investigated by many researchers (Najm & Ghoniem, 1994, Thibaut & Candel, 1998). Large vortical structures and turbulent flame speed play important roles in this kind of phenomenon. The latter is of essential importance since it controls the rate of mixture consumption.

The mean temperature field corresponding to the unstable flame is shown in Fig. 5. The temperature contours clearly exhibit a double-surface envelope flame anchored at the edges of the center body and the backward-facing step. This is in sharp contrast with the flame structure under stable operating conditions that shows only a single conical flame anchored to the centerbody. The overall flame length is substantially reduced. This situation renders the combustor more prone to instabilities according to the Rayleigh criterion (Rayleigh, 1945), since much heat release occurs within a short distance close to the chamber head-end (i.e., the acoustic anti-node point).

Unstable Flame Dynamics

When the inlet flow temperature exceeds a threshold value, an unstable flame is clearly observed, accompanied with large excursions of flow oscillations with frequencies corresponding the various characteristic dimensions of the chamber. In the present study, four dominant modes exist at 1795, 6582, 10970, and 21742 *Hz*. A simple acoustic analysis indicates that the 1795 *Hz* oscillation represents the first longitudinal (1L) wave in the main chamber, which agrees well with the experimental measurement of 1750 *Hz*. The 6582 *Hz* oscillation corresponds to the first longitudinal (1L) wave in the inlet annulus, and the 10970 *Hz* and 21742 *Hz* modes to the first tangential (1T) and the first radial (1R) waves in the main chamber, respectively. All of the calculated mode shapes match closely with the analytical solutions.

Vortex Shedding and Acoustics Interaction. As the flow expands from the inlet annulus to the chamber, strong shear layers arising from velocity differences are formed at the edges of the central body and backward-facing step. These shear layers and ensuing vortex shedding then interact with the acoustic field in the chamber to amplify the flow oscillations when the shedding and acoustics frequencies are close to each other.

A thorough review of large-scale structures in shear layers was given by Schadow & Gutmark (1992). A shear layer develops instability waves in its initial region. When the amplified waves reach a certain energy level, they roll up into vortices. The initial vortex shedding frequency, f_i, which is also called the most amplified frequency, can be scaled with the momentum thickness θ_0 of the initial shear layer and a characteristic velocity $\overline{U}$. The result yields a non-dimensional frequency or Strouhal number, $St_i = f_i \theta_0 / \overline{U}$, where $\overline{U}$ is defined as $(U_1 + U_2)/2$. For a turbulent shear layer, This Strouhal number is around 0.046 (Ho & Huerre, 1984). As vortices move downstream, they merge together to oscillate at the sub-harmonics of the initial vortex shedding frequency $f_i / N, (N = 2,3,4,...)$. In real flows, this process will be terminated at some point by the finite extent of the bounding stream and the frequency of the final sub-harmonic scaled on the maximum thickness attainable by the shear layer and also can be related to a characteristic dimension of the flow via another Strouhal number (Coats, 1996). For an axisymmetric jet, the Strouhal number can be written as: $St_j = f_j D / U_0$, where D is the jet exit diameter and U_0 is the jet exit velocity. The range of $St_j = f_j D / U_0$ was found to be between 0.25 and 0.5 and the frequency f_j is referred to as the preferred mode frequency. In the present study, the most amplified frequency is very close to the 1R mode (21742 *Hz* with $St_i \approx 0.05$) of the chamber and its second sub-harmonic frequency is very close to the 1T mode (10970 Hz). The preferred mode frequency (6582 *Hz* with $St_j = 0.433$) is very close to the 1L mode of the inlet annulus. These coincidences indicate that the resonance between vortex shedding and acoustic motions promotes excitations of the 1R and 1T mode of the main chamber and the 1L mode of the inlet annulus.

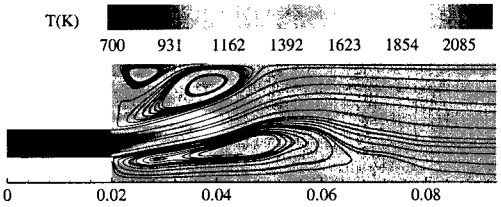

Fig. 5 Azimuthally averaged mean temperature contours and streamlines of unstable flame

Unstable Flame Evolution. The unstable flame dynamics can be elucidated by considering its interaction with the local oscillatory flowfield. Figure 6 presents the temperature evolution in the upstream part of the chamber on the $x-r$ and $r-\theta$ planes over one cycle of oscillation. The phase angle θ is referenced with respect to the acoustic pressure of the 1L mode at the chamber head-end. The entire process is dictated by the temporal evolution and spatial distribution of the cold flow entrainment into and mixing with the hot gases in the vortical structures in the chamber. During the pressure build-up stage (around $\theta = 0^o$), the increasing pressure and favorable pressure gradient near the dump plane facilitates the delivery of the fresh reactants into the chamber. Intensive heat release then follows after a short fluid mixing and chemical induction time. The resultant flow expansion pushes the flame outward and simultaneously blocks the inlet flow at the dump plane. Unburned mixture fragments may break up away from the main stream, and are convected downstream and generate local hot spots. In the next stage (around $\theta = 180^o$), the decreasing pressure and

adverse pressure gradient near the dump plane prevents the fresh mixture from traveling downstream to the chamber. The flame zone is thus shortened and becomes a little compact. It should be noted that the above description of the flame evolution is not precisely reflected in the temperature contours shown in Fig. 6 due to the various time delays involved in the process, but the qualitative trend remains valid.

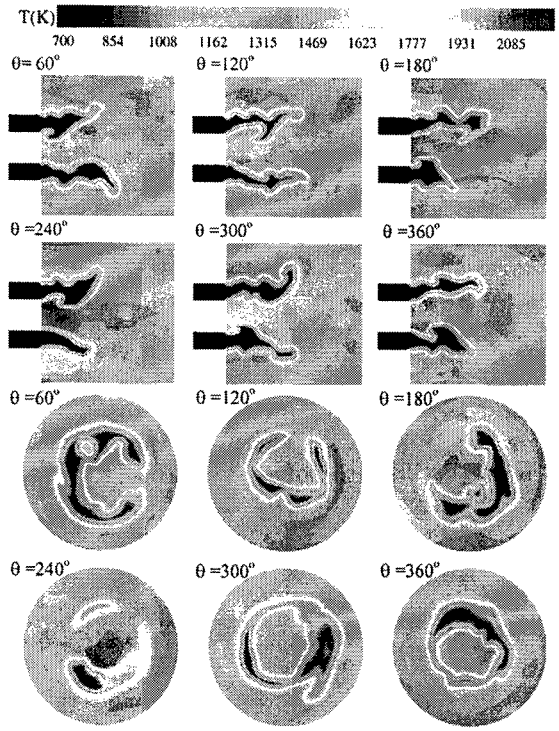

Fig. 6 Temperature contours on $x-r$ and $r-\theta$ planes (x=39.2*mm*) over one cycle of first longitudinal mode of oscillation.

Vortex and Flame Interaction. When the acoustic waves interact with the shear layer, the vortex size can be stabilized, depending on the matching of the frequencies between these two types of waves (Schadow and Gutmark, 1992). In the present case, as we discussed earlier, the most amplified frequency of the shear layer is close to the 1R mode (21742 Hz) of the chamber and the first sub-harmonic frequency $f_i/2$ =10455 *Hz* is close to the 1T mode (10970 Hz). Both the 1R and 1T modes are expected to interact intimately with the vortex shedding. However, the inlet exit, where the vortex shedding takes place, is located near the pressure nodal point of the 1R mode. Therefore, the matching between the 1T mode and the first sub-harmonic of the shear layer dominates the process of vortex shedding. Figure 7 shows the evolution of the vorticity and temperature fields during one cycle of the 1T mode of oscillation. The vortex shedding process is clearly visualized in the evolution of the vortex spiral, which gyrates around the centerline and propagates downstream. The flame surface is contorted and convoluted in phase with the vortex motion, further revealing the interaction between these two processes. Because the vortex shedding affects the shape of the flame front, it also changes the heat-release distribution. As a result, the acoustic motion in the chamber is closely coupled with the heat-release fluctuation.

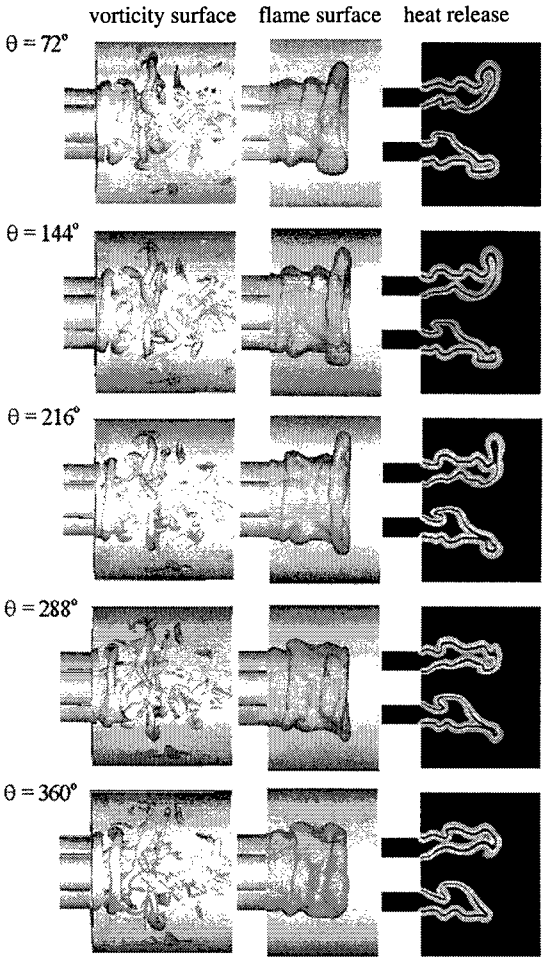

Fig. 7 Iso-vorticity surface of ω =75000 s^{-1} (R>0.02m is blanked), iso-thermal surface of T=1700 *K*, and normalized heat release contour over one cycle of first tangential mode of oscillation.

Coupling between Pressure and Heat Release. The mutual coupling between heat release and acoustic motions can be characterized using the Rayleigh parameter, $Ra(\mathbf{x})$, defined as the time-averaged product of the pressure oscillation $p'(\mathbf{x},t)$ and heat release fluctuation $q'(\mathbf{x},t)$:

$$Ra(\mathbf{x}) = \frac{1}{\tau}\int_{\tau} p'(\mathbf{x},t)q'(\mathbf{x},t)\,dt$$

where τ is the time period of oscillation. The acoustic oscillation is amplified if $Ra(\mathbf{x}) > 0$, or damped out if $Ra(\mathbf{x}) < 0$. Figure 8 shows the spatial distribution of the normalized Rayleigh parameter and the mean flame position (black line) in the x-r plane. A well organized distribution of the Rayleigh parameter is observed, with four asymmetrical dipoles located near the edge of the backward step and one near the edge of the center body. These dipoles, with larger positive values on the burnt side of the flame and smaller negative values on the unburnt side, arise from the wave-like distribution of heat release shown in Fig. 7. They are closely related to the local vortical motions. Our earlier work (Huang, et al. 2003a) indicates that the formation of these dipoles can be explained by considering the interaction between the flame and the local acoustic field. During the

pressure build-up stage with a positive pressure fluctuation, the flame zone is expanded. The flame front moves into the burnt region and results in a positive heat-release fluctuation on the burnt side and a negative heat-release fluctuation on the unburnt side. In the subsequent stage with a negative pressure fluctuation, the flame zone is reduced. The flame front propagates upstream into the unburnt region and produces a negative heat release fluctuation on the burnt side and a positive heat release on the unburnt side. In both stages, the heat-release fluctuation is in phase with the pressure oscillation in the burnt region and results in a positive $Ra(\mathbf{x})$; however, the situation becomes opposite in the unburnt region and consequently results in a negative $Ra(\mathbf{x})$.

In general, the Rayleigh parameter has a positive value in much of the volume in the flame zone. The acoustic field is favorably correlated with the unsteady heat release and extracts energy from combustion. The chamber exhibits a wide range of oscillation frequencies corresponding to the natural acoustic modes in various parts of the system.

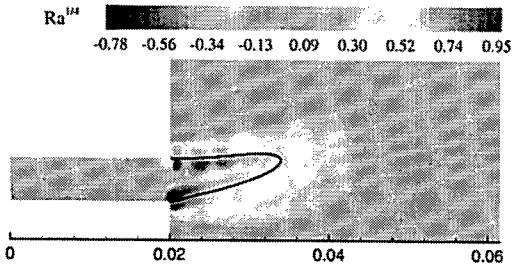

Fig. 8 Distribution of normalized Rayleigh's Parameter on $x-r$ plane; Black line: the mean flame position.

CONCLUSIONS

The unsteady flame dynamics in a lean-premixed, swirl-stabilized combustor has been studied using a large-eddy simulation technique along with a level-set flamelet library approach. Special attention was focused on the key mechanisms and operation parameters responsible for driving combustion instabilities. The results indicated that the inlet air temperature and equivalence ratio are the key parameters determining the stability characteristics of the combustor. A slight increase in the inlet flow temperature across the stability boundary leads to a transition from a stable to an unstable flame and consequently results in a sudden increase in acoustic flow oscillation. For an unstable flame, the thermal energy released from chemical reactions in the flame zone is fed to acoustic fluctuations in the chamber through a closed-loop feedback process, which includes the mutual coupling between acoustics excitation, vortex shedding, flame motion, and heat-release oscillation. Much information has been obtained to shed light to the fundamental mechanisms for initiating and sustaining combustion instabilities in gas-turbine engines.

REFERENCES

Apte, S. & Yang, V., 2001, "Unsteady Flow Evolution in Porous Chamber with Surface Mass Injection, Part 1: Free Oscillation," *AIAA J.*, 39:1577-1586.

Broda, J.C., Seo, S., Santoro, R.J., Shirhattikar, G. & Yang, V., 1998, "An Experimental Study of Combustion Dynamics of a Premixed Swirl Injector," *Proc. Combust. Inst.*, 27:1849-1856.

Coats, C.M., 1996, "Coherent Structures in Combustion," *Prog. Energy Combust. Sci.*, 22: 427-509.

Correa, S.M., 1993, "A Review of NO_X Formation Under Gas-Turbine Combustion Conditions," *Combust. Sci. Tech.*, 87:329.

Erlebacher, G., Hussaini, M.Y., Speziale, C.G. & Zang, T.A., 1992, "Toward the Large Eddy Simulation of Compressible Turbulent Flows," *J. Fluid Mech.*, 238:155-158.

Ho, C.M. & Huerre, P., 1984, "Perturbed Free Shear Layer," *Ann. Rev. Fluid Mech.*, 16, 365-424.

Huang, Y., Sung H.G., Hsieh S.Y. & Yang, V., 2003a, "LES of Combustion Dynamics of a Lean-Premixed Swirl-Stabilized Injector," Submitted to *J. Propul. Power.*

Huang, Y., & Yang, V., 2003b, "Bifurcation of Flame Structure in a Lean-Premixed Swirl-Stabilized Combustor: Transition From Stable to Unstable Flame," *Third Joint Meeting of the U.S. Sections of The Combustion Institute.*

Johnson, C.E., Neumeier, Y., Lieuwen, T.C. & Zinn, B.T., 2000, "Experiment Determining of Stability Margin of a Combustor Using Exhaust Flow and Fuel Injection Rate Modulations," *Proc. Combust. Inst.*, 28: 757-763.

Knoop, P., Culick, F.E.C. & Zukoski, E.E., 1997, "Extension of the Stability of Motions in a Combustion Chamber by Nonlinear Active Control Based on Hysteresis," *Combust. Sci. Tech.*, 123:363-376.

Kurdyumov, V.N., Fernandez, E. & Linan, A., 2000, "Flame Flashback and Propagation of Premixed Flames Near a Wall," *Proc. Combust. Inst.*, 28:1883-1889.

Lee, J.G., Kim, K. & Santavicca, D.A., 2000, "Measurement of Equivalence Ratio Fluctuation and Its Effect on Heat Release During Unstable Combustion," *Proc. Combust. Inst.*, 28:739-746.

Lefebvre, A. H., 1995, "The Role of Fuel Preparation in Low-Emission Combustion," ASME *J. Eng. Gas Turbines Power*, 117:617-654.

Lieuwen, T. & Zinn, B.T., 1998, "The Role of Equivalence Ratio Oscillation in Driving Combustion Instabilities in Low Nox Gas Turbines", *Proc.Combust Inst.*, 27:1809-1816

Najm, H.N. & Ghoniem, A.F., 1994, "Coupling Between Vorticity and Pressure Oscillations in Combustion Instability," *J. Propul. Power*, 10:769-776.

Oefelein, J.C. & Yang, V., 1998, "Modeling High-Pressure Mixing and Combustion Processes in Liquid Rocket Engies," *J. Propul. Power*, 14:843-857.

Pitsch, H. & Duchamp, de lageneste L., "large eddy simulation of premixed turbulent combustion using a level-set approach", *Proc. Combust. Inst.*, 29 (2002)

Rayleigh, J.W.S., 1945, *The Theory of Sound*, Vol. II, Dover, New York .

Seo, S., 1999, "Parametric Study of Lean Premixed Combustion Instability in a Pressurized Model Gas Turbine Combustor," *Ph.D. Thesis*, The Penn State University.

Swanson, R.C. & Turkel, E., 1992, "On Central-Difference and Upwind Schemes," *J. Comput. Phys.*, 101:292-306.

Thibaut, D. & Candel, S., 1998, "Numerical Study of Unsteady Turbulent Premixed Combustion: Application to Flashback Simulation," *Combust. Flame*, 113:53-65.